https://doi.org/10.5194/essd-2025-131
Preprint. Discussion started: 12 March 2025

Open Access Earth System Science Data Discussions

Phytoplankton coastal-offshore monitoring by the Strait of Dover at high spatial resolution: the DYPHYRAD surveys

Zéline Hubert[1,★], Aurélie Libeau[1,★], Clémentine Gallot[1,2], Vincent Cornille[1,3], Muriel Crouvoisier[1], Éric Lécuyer[1], and Luis Felipe Artigas[1]

[1]Université Littoral Côte d'Opale, Université de Lille, CNRS, UMR 8187, LOG, Laboratoire d'Océanologie et de Géosciences, 62930, Wimereux, France
[2]Mediterranean Institute of Oceanography (MIO), Campus de Luminy, 163 Av. de Luminy, 13288 Marseille cedex 9, France
[3]Ifremer, Unité Littoral, Laboratoire Environnement et Ressources, 150 quai Gambetta, 62321 Boulogne-sur-mer, France
★These authors contributed equally to this work.

Correspondence: Zéline Hubert (zeline.hubert@univ-littoral.fr), Aurélie Libeau (aurelielibeau44@gmail.com), and Luis Felipe Artigas (felipe.artigas@univ-littoral.fr)

Abstract. Long-term monitoring of phytoplankton communities is essential for understanding the functioning and evolution of marine systems. This paper presents a decadal dataset on phytoplankton observations conducted along a coastal-offshore transect by the Strait of Dover, at fine spatial resolution, using an automated *in vivo* approach. Nine stations (∼ 1 km apart) were sampled off the Slack estuary, representing the northern limit of the Marine Protected Area of "Picard Estuaries and Opal Seas" (EPMO). Since 2012, phytoplankton functional groups were characterized *in vivo* in sub-surface waters using multi-spectral fluorometry (Fluoroprobe, bbe Moldaenke, Gmbh) and single-cell optical analysis with a pulse shape-recording flow cytometer (CytoSense and CytoSub, Cytobuoy b.v., Netherlands). Total phytoplankton biomass was estimated via chlorophyll *a* extraction and *in vivo* fluorescence. Spectral and functional groups were quantified in terms of abundance, size, and estimated chlorophyll *a* in surface waters. Weekly sampling resolution allowed to address the community composition in order to disentangle short-term, fine spatial, seasonal, and inter-annual variability. Additionally, biogeochemical and hydrological variables—temperature, salinity, Photosynthetically Active Radiation (PAR), and nutrients (nitrate, nitrite, phosphate, silicate) were systematically measured. Over 11 years, the survey generated 1,835 samples from 268 dates, averaging 167 samples per year across 24 cruises. This unique dataset provides valuable insights into phytoplankton dynamics and environmental drivers in a temperate coastal system. Free access to the dataset can be found at https://www.seanoe.org/data/00933/104524/ (Hubert et al., 2025).

1 Introduction

Phytoplankton are central to marine ecosystems, driving much of the primary production (Rousseaux and Gregg, 2014) and forming the foundation of most marine food webs (Berglund et al., 2007). Their contribution to biogeochemical cycles, including their role in climate regulation through the biological pump, makes them a critical component of oceanic systems (Giering and Humphreys, 2017). As their dynamics are closely linked to environmental variations, phytoplankton are increasingly used as biological indicators for assessing marine ecosystem health (Bierman et al., 2011; Rombouts et al., 2019).

https://doi.org/10.5194/essd-2025-131
Preprint. Discussion started: 12 March 2025

Understanding these dynamics is particularly important in regions subject to significant anthropogenic pressures and environmental variability, such as Pas-de-Calais (Strait of Dover). The Strait of Dover, which connects the English Channel and the North Sea, is characterized by intense maritime activity (Wang et al., 2023), heavy fishing pressure (Girardin et al., 2015), and the influence of adjacent industrialized areas (e.g., ports, industrial activities) and agricultural regions, as well as runoff from local estuaries. The hydrodynamic regime characterized by strong currents, a macro-tidal regime as well as remote and local estuarine inputs significantly shape phytoplankton communities in this region (Desmit et al., 2020; Kang et al., 2021; Salmaso and Tolotti, 2021). This area is also subject to regular blooms of *Phaeocystis globosa* (Astoreca et al., 2009; Lefebvre et al., 2011; Breton et al., 2022; Skouroliakou et al., 2022, 2024), a haptophyte species whose genus is known for its wide distribution and potential ecological impact (Lancelot et al., 1994, 1998; Medlin and Zingone, 2007; Li et al., 2022). While non-toxic in the Eastern English Channel and the North Sea (Cadée and Hegeman, 2002), these blooms are considered undesirable due to their tendency to form dense gelatinous colonies and foam layers, particularly during periods of strong winds (Lefebvre and Delpech, 2004). This phenomenon affects water density, potentially disrupts both benthic and pelagic ecosystems (Karasiewicz et al., 2018), and has occasionally resulted in human fatalities (Peperzak and van Wezel, 2023). Historically, phytoplankton monitoring in this region has been conducted within French National Observation Services (SNO) through long-standing networks such as SRN-REPHY (https://manchemerdunord.ifremer.fr/Environnement/LER-Boulogne-sur-Mer/Surveillance-et-Observation/Reseaux-nationaux, last access: 6th March 2025), SOMLIT (https://www.somlit.fr/wimereux/, last access: 6th March 2025), and PhytOBS (https://www.phytobs.fr/Stations/Boulogne, last access: 6th March 2025), providing valuable and accessible data on chlorophyll *a* concentration and microphytoplankton diversity. However, these programs are set for monthly to fortnightly collection on a reduced number of stations, and consider mainly microscopic counts of micro- and some nanophytoplankton species, even though, since 2009, pico- and nanoplankton abundance were addressed by benchtop flow cytometry on fixed samples at some stations. Advances in automated monitoring technologies enable more detailed observations of phytoplankton communities, providing insights across the entire size spectrum from a single *in vivo* sample and allowing data acquisition at higher spatial and temporal resolutions. This study presents the DYPHYRAD (DYnamics of PHYtoplankton on RADiale of the Saint-Jean Bay) dataset, encompassing 11 years (2012–2022) of automated, high-resolution monitoring of phytoplankton communities on a coastal-offshore transect in the Strait of Dover. Weekly surveys were conducted along a coastal-offshore transect, integrating data from a multi-spectral fluorometer (Fluoroprobe, bbe Moldaenke, Gmbh) and an automated pulse-shape recording flow cytometer (CytoSense and CytoSub, Cytobuoy b.v., Netherlands). Combined with hydrological and biogeochemical measurements, this dataset provides a comprehensive view of phytoplankton dynamics (including abundance, scatter, fluorescence, chlorophyll *a* and pigments content) at a fine spatial scale. By making this dataset available in accordance with FAIR principles (Findable, Accessible, Interoperable, Reusable), this research aims to support further studies on seasonal and inter-annual variations, long-term trends, and the impacts of environmental drivers on phytoplankton communities. In doing so, it offers valuable contributions to understanding the health and resilience of marine coastal ecosystems under increasing anthropogenic and climate pressures.

https://doi.org/10.5194/essd-2025-131
Preprint. Discussion started: 12 March 2025

2 Aim of the data collection

Long-term observation data are essential for understanding the functioning and state of marine ecosystems and for providing environmental managers with the information needed to mitigate anthropogenic pressures on marine ecosystems. By integrating these data into public policy indicators of ocean health and biodiversity, effective measures can be devised to preserve marine environments. The DYPHYRAD surveys focus on understanding the dynamics of marine phytoplankton and their associated environmental variables across the distinct water masses of the Strait of Dover. These measurements complement national and regional monitoring networks (SOMLIT, REPHY, PhytOBS) by providing higher sampling frequency (weekly) and finer spatial resolution (∼ kilometer scale). Since 2022, this monitoring program has been recognized as an observation of interest for the French research and manager's community of the national Coastal and Littoral French Research Infrastructure (ILICO, i.e. Infrastructure de recherche LIttorale et CÔtière).

3 Material and Methods

3.1 Study site

The Eastern English Channel (EEC) is a shallow region, with depths not exceeding 50 meters, and is influenced by a macro- and mega-tidal regime that can exceed 8 meters. These tidal forces, combined with the area's bathymetry, variable wind regimes, and proximity to the Pas-de-Calais (Strait of Dover), generate strong hydrodynamics, with average current velocities reaching 1 m s^{-1} (Lazure and Desmare, 2012; Thiébaut and Sentchev, 2016). The predominant drift of these currents towards the Northeast intensifies mixing and stratification processes within the water column, significantly affecting the physico-chemical characteristics of the region (e.g., mixing/stratification) (Lazure and Desmare, 2012). Coastal waters in the EEC are further enriched by nutrient inputs from numerous watersheds, including the Somme, Authie, Canche, Liane, Wimereux, and Slack estuaries along the Picardy and Opale coasts (Bentley et al., 1993). These influences lead to the formation of a Region of Freshwater Influence (ROFI), where freshwater outflows from these estuaries create a distinct coastal water mass that remains along the coast, separated from the offshore waters by a tidal front (Brylinski et al., 1991). This 'coastal flow' presents unique characteristics and interacts dynamically with adjacent water masses.

The DYPHYRAD transect is strategically located in this complex environment, near the Strait of Dover, at the northern edge of the Picardy Estuaries and Opal Sea Marine Protected Area (EPMO). Positioned off the Slack estuary, the transect captures the combined influence of several estuaries within the EPMO. By extending from the offshore to the coast, the transect allows for monitoring, at high spatial resolution, water bodies that are often very close but have distinct properties. This location is crucial for long-term monitoring, as it allows for the study of cumulative estuarine effects and the interactions between coastal and offshore water masses. The DYPHYRAD monitoring offers weekly observations that enhance our understanding of the hydrodynamics and environmental variability in this ecologically and economically important region.

https://doi.org/10.5194/essd-2025-131
Preprint. Discussion started: 12 March 2025

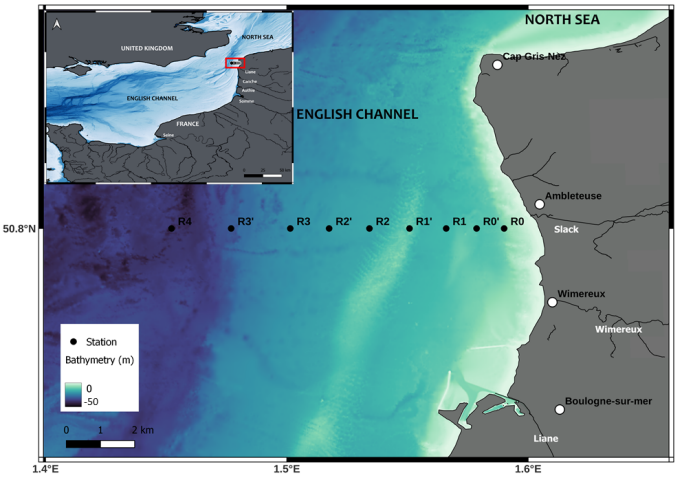

Figure 1. Map of the study area (indicated by the red square on the high scale map) and location of DYPHYRAD stations. The bathymetry data come from SHOM 2015 and 2016 (https://diffusion.shom.fr/donnees/bathymerie/mnt-cotier-pas-de-calais.html).

3.2 Sampling strategy

From 2012 to 2022, weekly sampling and measurements were conducted along a coastal-offshore transect by the Strait of Dover aboard the research vessel "*Sepia II*" (CNRS INSU, French Oceanography Fleet-FOF). While the goal was to maintain a regular weekly sampling schedule, the actual frequency was occasionally disrupted by adverse weather conditions (e.g., during the winter of 2015), unexpected logistical issues, and the COVID-19 pandemic, including a prolonged interruption during the lockdown in the spring of 2020. Details on the frequency of cruises and the number of stations sampled are summarized in Fig. 2. The transect spans 9.7 kilometers, consisting of nine sub-surface sampling stations from R4 (50°8' N, 1°45'22 E) offshore to R0 (50°8' N, 1°59' E) nearshore (Fig. 1; Appendix A1). This transect captures key environmental gradients, such as those driven by estuarine inputs and hydrodynamic mixing. High-resolution hydrological measurements, including temperature, salinity, Photosynthetically Active Radiation (PAR), *in vivo* chlorophyll *a* fluorescence, and turbidity, were collected throughout the water column at each station using a multi-parameter probe. Seawater samples were collected using Niskin bottles. Dissolved inorganic nutrients (nitrite, nitrate, phosphate, silicate) were measured from surface water samples at the main stations R0, R1, R2, R3, and R4. Discrete samples were used to measure biological variables, including *in vivo* chlorophyll *a* fluorescence, extracted chlorophyll *a*, and phaeopigments. Phytoplankton spectral and functional diversity was assessed at all nine stations using a combination of optical and fluorometric approaches on surface *in vivo* samples. Between 2016 and 2020, extra daily sampling cruises were conducted at three key stations (R1, R2, and R4) to capture high-frequency dynamics during periods of particular interest. These additional surveys supported a range of analyses, including phytoplankton microscopy and molecular characterization of microbial diversity through metabarcoding techniques (Fig. 2; Skouroliakou et al., 2022, 2024).

https://doi.org/10.5194/essd-2025-131
Preprint. Discussion started: 12 March 2025

Open Access Earth System Science Data Discussions

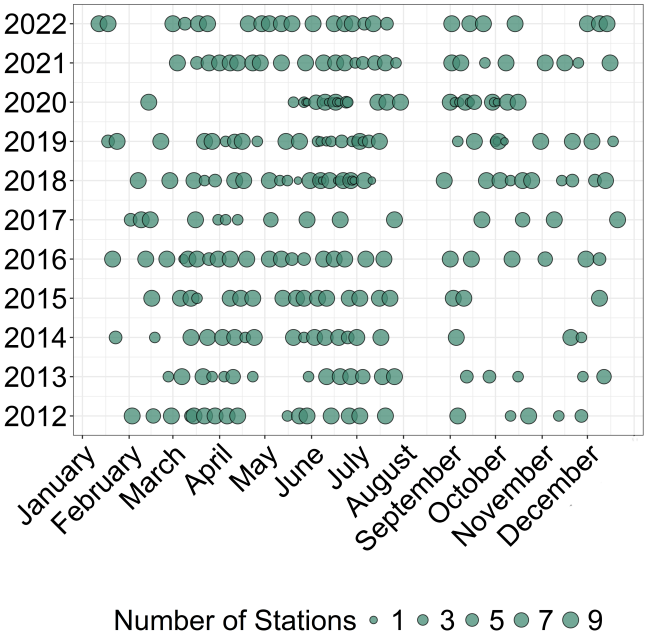

Figure 2. Distribution of DYPHYRAD sampling over years (2012-2022). The dot size represent the number of monitored stations for each discrete sampling.

3.3 Hydrological and biogeochemical variables

Depth, temperature, salinity, PAR, and fluorescence were measured across the water column at each sampling point using a CTD profiler (SBE 19+ and SBE 25, SeaBird Ltd, United States) equipped with a WETStar Fluorometer (SeaBird Ltd, Etats-Unis). Sub-surface values were calculated as the average of measurements taken between 1 and 2 meters deep. Additional measurements of temperature and conductivity/salinity were acquired by a manual probe on the surface and, since 2017, a thermo-salinograph (TSG) installed on the research vessel "*Sepia II*", which continuously samples seawater at approximately 2.5 meters deep via an onboard pump. While only CTD-derived data are presented in this study due to their coverage of the full study period, manual probe and TSG data are available for complementary analyses.

Concentrations of dissolved inorganic nutrients (NO^{2-}, NO^{3-}, SiO_2 and H_3PO_4) were collected at the sub-surface using Niskin bottles. The samples were transferred to sterile 50 mL PVC flasks, then analyzed on the day of collection or frozen at -20 °C following the guidelines of Aminot and Kérouel (2007). The concentrations of nutrients were quantified using an autoanalyzer (AutoAnalyzer ALLIANCE SpA, Italy, then, since 2016, AA3 HR AutoAnalyzer, SEAL Analytical GmBH, Germany). The analyses followed the SOMLIT protocol, based on the methodology described by Aminot and Kérouel (2007).

In the laboratory, water samples for chlorophyll *a* and phaeopigment analyses kept in the dark inside a cooler, then were filtered onto GF/C 47 mm Whatman glass fiber filters and stored at -80 °C until processing. Pigments were extracted *in vitro*

https://doi.org/10.5194/essd-2025-131
Preprint. Discussion started: 12 March 2025

using 90 % acetone. Filters were ground, refrigerated at 4 °C overnight, and analyzed using a Turner Designs benchtop fluorometer (10-AU Field Fluorometer, Turner Designs Ltd., United States). Fluorescence emission at 685 nm was measured after excitation at 440 nm, both before and after acidification with 0.3 mol L^{-1} HCl, following the protocol of Holm-Hansen et al. (1965). Chlorophyll *a* and phaeopigment concentrations were estimated using the equations of Lorenzen (1967). The percentage of chlorophyll *a* relative to total pigments was calculated, providing a proxy for the proportion of active pigments. Calibration of the fluorometer with pure chlorophyll *a* was performed annually to ensure measurement accuracy.

3.4 Automated *in vivo* phytoplankton measurements

3.4.1 Total chlorophyll *a* estimated by *in vivo* mono-spectral fluorometry

Upon returning to the laboratory, *in vivo* fluorescence was measured immediately on 50 mL water samples using a Turner Designs benchtop fluorometer (10-AU Field Fluorometer, Turner Designs Ltd, USA). Measurements captured the maximum, minimum, and stabilized mean fluorescence at 685 nm following excitation at 440 nm, which provided an estimate of total chlorophyll *a* fluorescence. Checking instrument stability was performed using a dedicated solid standard to ensure measurement accuracy and reliability.

3.4.2 Phytoplankton spectral (pigmentary) groups addressed by *in vivo* multi-spectral fluorometry

In the laboratory, each sample kept in the dark in a cooler, was analyzed within maximum four hours of collection using a multi-spectral fluorometer (FluoroProbe, FLP, bbe Moldaenke, Gmbh). The FluoroProbe emits light at five wavelengths (470, 525, 570, 590 and 610 nm) to differentiate among four phytoplankton pigmentary groups (Fig. 3) and at 370 nm (UV LED) to correct for fluorescence contributions from yellow substances. Operated in benchtop mode, the instrument estimates the concentration or relative contribution up to four phytoplankton pigmentary groups in total chlorophyll *a* equivalents (μg chl-*a* Eq L^{-1}).

Spectral groups were distinguished according to the relative fluorescence of chlorophyll *a* at 680 nm after excitation of chlorophyll *a* and accessory photosynthetic pigments. This differentiation utilized a manufacture's algorithm derived from monoculture fingerprints of the main pigmentary groups (Beutler et al., 2002). The instrument can also deliver total chlorophyll *a* estimates (sum of all detected concentrations of algae classes).

Only four spectral groups can be addressed at a time. However, new fingerprints can be recalculated with the bbe++ or FluoroProbe software in Expert mode. Algae classes defined by the manufacturer were "blue-green" (phycocyanin-rich: cyanobacteria), "green algae" (rich in chlorophyll *a* and *b* as chlorophytes and also part of the haptophyte signal; Houliez et al., 2012), "brown algae" corresponding to diatoms (xanthophyll, most dinoflagellates and part of the haptophyte signal), and "red-mix algae" (phycoerythrin-rich: mainly cryptophytes, cyanobacteria). Groups were estimated by applying an algorithm (Beutler et al., 2002) correcting the residual fluorescence of dissolved organic matter ("yellow substances") and the turbidity (% of light transmission). Initially, the FluoroProbe TS-16-16 was supplied with fingerprints for "brown algae", "blue-green", "green algae" and "red-mix algae" (original fingerprints). In order to better discriminate the haptophyte *Phaeocystis*, a new finger-

https://doi.org/10.5194/essd-2025-131
Preprint. Discussion started: 12 March 2025

print was recorded in 2012 by Houliez et al. (2012) using natural coastal water dominated by this species. Since 2021, the manufacturer introduced a generic haptophyte fingerprint, which was incorporated into the *Isochrysis* fingerprint and added on the TS-22-15 FluoroProbe in 2021. Moreover, the manufacturer's name for "brown algae" is Diatoms and for "mix-red" is Cryptophyta. Thus, even though we do not agree on this nomenclature, for FAIR principles we have kept in the Database and this presentation.

Two different FluoroProbe devices were used during the 11 years of measurement, with simultaneous period: TS-22-15 (2012-2016 and 2021-2022) and TS-16-16 (2012-2022). The devices were set to measure during 2-3 minutes, with one acquisition every 3 seconds. These measurements were then averaged for each sample. Over 11 years, a total of 1,253 samples were analyzed by the TS-22-15 and 1,835 by the TS-16-16. Outliers were determined on the basis of the correlation between total *in vivo* chlorophyll *a* fluorescence measured on the 10-AU Field Fluorometer, and the FLP total chlorophyll *a* estimated by the FluoroProbe. A total of 43 values were considered *a posteriori* as outliers (Fig. 4). These values were not included in the following study. There was a strong correlation between total *in vivo* chlorophyll *a* fluorescence on the 10-AU TD fluorometer measurements and FLP total chlorophyll *a* estimations: $R = 0.85$ for TS-16-16, $R = 0.89$ for TS-22-15 (p-value < 0.001) (Fig. 4) and after removing outliers $R = 0.93$ (p-value < 0.001) for TS-22-15.

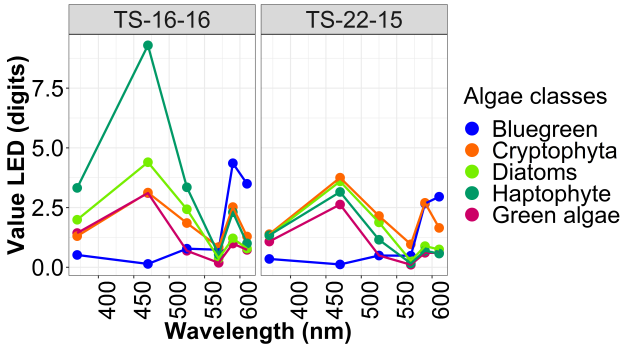

Figure 3. Different fingerprints of algae classes for each Fluoroprobe : TS-16-16 and TS-22-15.

3.4.3 Abundance and biomass of phytoplankton optical (functional) groups addressed by Automated Flow Cytometry

All samples were analysed *in vivo* after maximum 4 hours of dark conservation in a cooler, followed by storage at 4 °C in a refrigerator. Analysis was performed using an automated pulse shape-recording flow cytometer (CytoSense/CytoSub). This instrument provides optical measurements at the particle level. It covers the entire phytoplankton size range from 0.1 to 800 μm width and allows to obtain abundance, size, structure and pigmentation data at the particle scale due to the use of 5 optical signals. Size and structure of pigmented cells and colonies are characterised by scattering at large and small angles (FWS and SWS). The other three signals provide information on the pigment content of the cells and their potential physiological state through the emission of red fluorescence (chlorophyll *a*, FLR, 668-734 nm), orange fluorescence (phycobiliproteins (Phycoerythrin and Phycocyanin), FLO, 604-668 nm) and yellow fluorescence (Phycoerythrin, FLY, 536-601 nm) (Fontana et al.,

https://doi.org/10.5194/essd-2025-131
Preprint. Discussion started: 12 March 2025

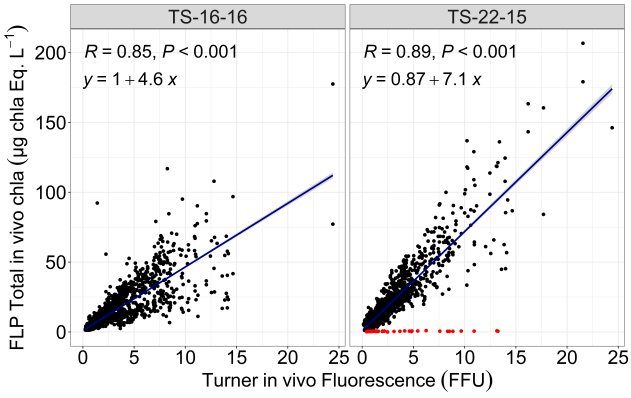

Figure 4. Outliers detection for Fluoroprobe TS-16-16 and TS-22-15. R value represent the coefficient of correlation estimated using linear regression model (blue line). y represent the equation of each blue line. The associated p-values are also provided (P). The red dots correspond to values identified as outliers.

2014; Haraguchi et al., 2017; Fragoso et al., 2019). Two protocols were used for each sample: one for small cells, called "Pico protocol" (low detection threshold, low pump speed - 5 μL s^{-1}, short duration - 5 minutes) and one for larger cells or "Micro protocol" (higher detection threshold, faster - between 10 and 13 μL s^{-1}, longer duration - 8 minutes). Using the dedicated manual classification software (CytoClus4, Cytobuoy b.v., Netherlands), 6 main functional groups were characterized, according to the interoperable vocabulary from Thyssen et al. (2022), already described in the area: OraPicoProk or *Synechococcus*-like cells, RedPico or picoeukaryotes, RedNano or nanoeukaryotes, HsNano or Coccolithophore-like cells, OraNano or Cryptophyte-like cells and RedMicro (diatoms and dinoflagellates bigger than 20 μm, haptophyte colonies, pigmented ciliates, filamentuous cyanobacteria (not present in our site so far; Fig. 5)). The files were analyzed by a single person to minimize interpretation bias. Fluorescent polyester beads of 1 and 3 μm (Fluospheres Carboxylate-Modified, Invitrogen, 1.0 μm, yellow-green fluorescent and Sphero brand beads, Spherotech Inc., 3.0-3.4 μm, bright intensity) were also analyzed regularly to monitor measurement quality and help discriminate size classes.

It should be noted that different Cytosense and CytoSub devices were deployed throughout the years from different funding opportunities and projects, in part to stay up-to-date with evolving technologies and also to diversify their *in situ* deployments. Sometimes, instruments were shipped on campaigns, implemented in fixed autonomous measuring stations or sent to maintenance, which explains the use of different machines depending on the period. During this 11-year time series, the following four instruments were used: CS-2007-15; CS-2016-78; CS-2019-93 and CS-2019-94 (Fig. 6). At each machine changeover, common samples were analyzed to ensure that the measurements were robust over time.

https://doi.org/10.5194/essd-2025-131
Preprint. Discussion started: 12 March 2025

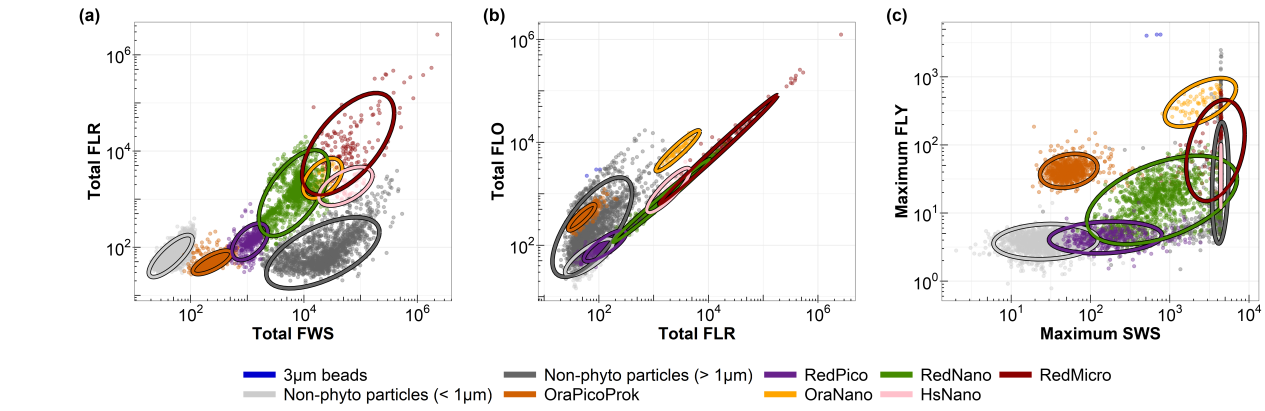

Figure 5. Cytograms showing the main groups defined during the 11 years along the DYPHYRAD transect (e.g., R0 station on March 24, 2024), characterizing the main phytoplankton groups: (a) total red fluorescence (Total FLR) vs total forward scatter (Total FWS) for the discrimination of red fluorescence groups and size class, (b) total red fluorescence (Total FLR) vs total orange fluorescence (Total FLO) for the discrimination of orange fluorescence groups, (c) maximum yellow fluorescence (Maximum FLY) vs maximum sideward scatter (Maximum SWS) for the discrimination of *Coccolithophoridaea* (HsNano). Ellipses on the graphs are calculated from a *t*-distribution at 95 % confidence level, aiding in accurate delineation of the respective phytoplankton groups.

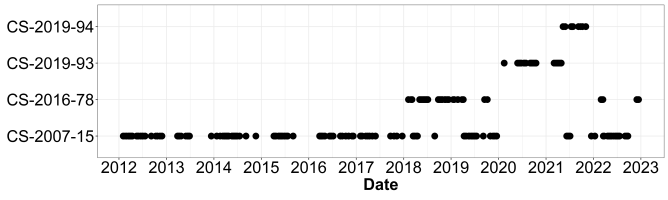

Figure 6. Diagram of the use of different flow cytometers during the DYPHYRAD time-series. The dots indicate the cytometer used for each discrete sampling over time.

3.5 Quality control

Only data with a good quality code are presented in this study and are available in the data set, according to Argo quality control (www.somlit.fr/codes-qualite/; Wong et al., 2019). Based on the characteristics of each device, the detection limits of each variable are described in Table 1.

4 Results and discussion

4.1 Hydrological and biogeochemical variables

The DYPHYRAD transect is characterized by a marked seasonal cycle and a spatial gradient from the coast to the offshore (Fig. 7). Sea Surface Temperatures (SST) were relatively homogeneous along the longitudinal gradient of the transect, but were

https://doi.org/10.5194/essd-2025-131
Preprint. Discussion started: 12 March 2025

Open Access Earth System Science Data Discussions

Table 1. Summary of detection limit value for each parameters. The notation "-" means that there was not any detection limit.

Parameters	Detection limit
Temperature (°C)	-
Salinity (PSU)	-
PAR (μmol s^{-1} m^{-2})	-
Fluorescence (FFU)	-
Nitrite (μmol L^{-1})	0.03
Nitrate (μmol L^{-1})	0.05
Phosphate (μmol L^{-1})	0.02
Silicate (μmol L^{-1})	0.05
Chlorophyll *a* (μg L^{-1})	0.02
TD-10AU *In vivo* fluorescence (FFU)	-
FluoroProbe chl-a (μg chl- *a* Eq. L^{-1})	0-200
Cell abundance (particule L^{-1})	10^2 to 10^{10}

strongly influenced by seasonal cycle (Fig. 7A; Lefebvre and Ambiaud, 2017). Solar radiation, contrarily, showed small-scale disparities, partly linked to potential coastal turbidity and to the sampling method strategy (from offshore to the coast; Fig. 7C).

Winters during the period from 2012 to 2022, were characterized by low temperatures ranging from 5.03 °C in 2013 to 13.06 °C in 2022 (mean: 8.43 °C, Fig. 8) and relatively low levels of solar radiation, ranging from 3 μmol s^{-1} m^{-2} in 2021 to 528 μmol s^{-1} m^{-2} in 2017 (mean: 130 μmol s^{-1} m^{-2}, Fig. 8). Spring is a transition period during which SST began to rise, with values ranging from 5.21 °C in 2013 to 15.99 °C in 2017 (mean 9.79 °C), and a PAR ranging from 12 in 2014 to 1209 μmol s^{-1} m^{-2} in 2015 (mean: 348 μmol s^{-1} m^{-2}).

Surface waters warmed considerably during the summer, with temperatures ranging from 11.70 °C in 2013 to 20.57 °C in 2022 (mean: 16.26 °C). This warming was controlled by solar radiation, which was relatively high in summer, ranging from 19 in 2015 to 1360 μmol s^{-1} m^{-2} in 2022 with an average value of 487 μmol s^{-1} m^{-2}. Autumn is characterized by a decrease in average solar radiation (234 μmol s^{-1} m^{-2}) despite values that may still be close to those of summer (maximum: 1722.56 μmol s^{-1} m^{-2} in 2019). A similar pattern is also observed for surface water temperatures (between 9.90 °C in 2016 and 20.66 °C in 2022; mean of 16.30 °C).

Over these 11 years, SST have increased, particularly in winter. This increase in SST was in line with previous observations in the area and on a global scale (Saulquin and Gohin, 2010; Auber et al., 2017; Ruela et al., 2020). The warmest year of our time series for all seasons was 2022. In terms of solar radiation, the greatest variation was observed in summer 2022, with mean solar radiation considerably higher than in the other years. This follows the heat wave observed during the summer of 2022, with average sea surface temperatures throughout France between +1.3 and +2.6 °C above the long-term average (1982-2011), linked to high air temperatures and above-average surface solar radiation and below-average total cloud cover (Guinaldo et al., 2023).

https://doi.org/10.5194/essd-2025-131
Preprint. Discussion started: 12 March 2025

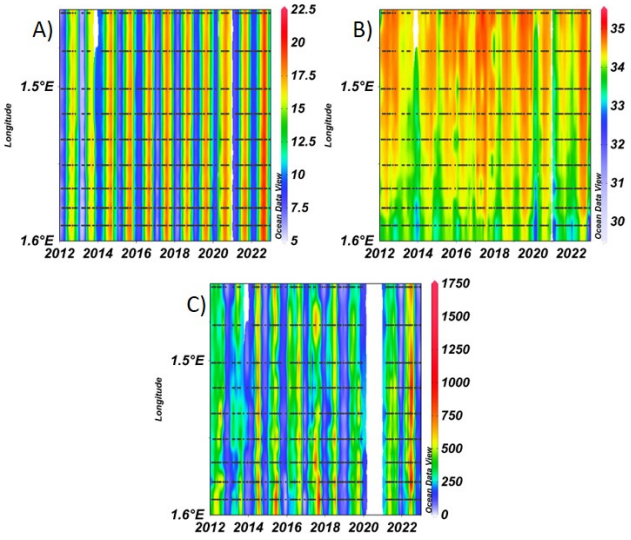

Figure 7. Spatial variability of surface hydrological variables over time: (A) temperature (°C), (B) salinity (PSU) and (C) PAR (μmol s^{-1} m^{-2}) along coastal-offshore DYPHYRAD transects.

As for salinity, the area was not characterized by a seasonal cycle (Lefebvre and Ambiaud, 2017), with relatively slight variations between spring (mean: 34.13 PSU), summer (mean: 34.35 PSU) and autumn (mean: 34.29 PSU). However, within these seasons, there are major disparities from one year to the next, with more widespread extreme values (min: 32.23 in spring 2021 to 34.69 PSU in summer 2017; max: 33.97 in spring 2020 to 35.11 PSU in spring 2017). Salinity values were highest at the offshore stations and have been marked by strong desalination in 2020 (Fig. 7B). The month of February 2020 was marked by major storms ("Ciara", "Inès" and "Dennis") which influenced the wind and therefore the mixing of the water column as well as freshwater inflows (Galvin, 2022). EEC is characterized by the influence of strong freshwater flows, linked to the many estuaries along the French coast, and by periods of heavy precipitation (Taylor et al., 1981). Only winter season stood out, with lower values ranging from 29.65 to 34.97 PSU with a mean value of 33.9 PSU (Fig. 8). Winter salinity variations seem to occur over several years, with cycles of high values (for the years 2012, 2015 to 2017 then 2021 and 2022) and low values (2013, 2014, 2018, 2019 and 2020).

Spatially, all nutrients exhibited pronounced spatial and temporal heterogeneity (Fig. 9). However, nitrates displayed a strong coastal-offshore gradient. This gradient can be attributed to the influence of rivers and rainfall on the concentration of dissolved inorganic nitrogen along the French coast (Dulière et al., 2019). The Strait of Dover is subject to pronounced seasonal nutrient cycles, and this phenomenon is especially marked in the coastal zone due to inputs, particularly from the French coast (Bentley et al., 1993). These inputs follow the "river flow" ROFI and include brackish waters from the Somme to the Slack estuary (Brylinski et al., 1991), characterized by high concentration of phosphate, silicate, nitrate and nitrite concentrations during winter (Fig. 10).

https://doi.org/10.5194/essd-2025-131
Preprint. Discussion started: 12 March 2025

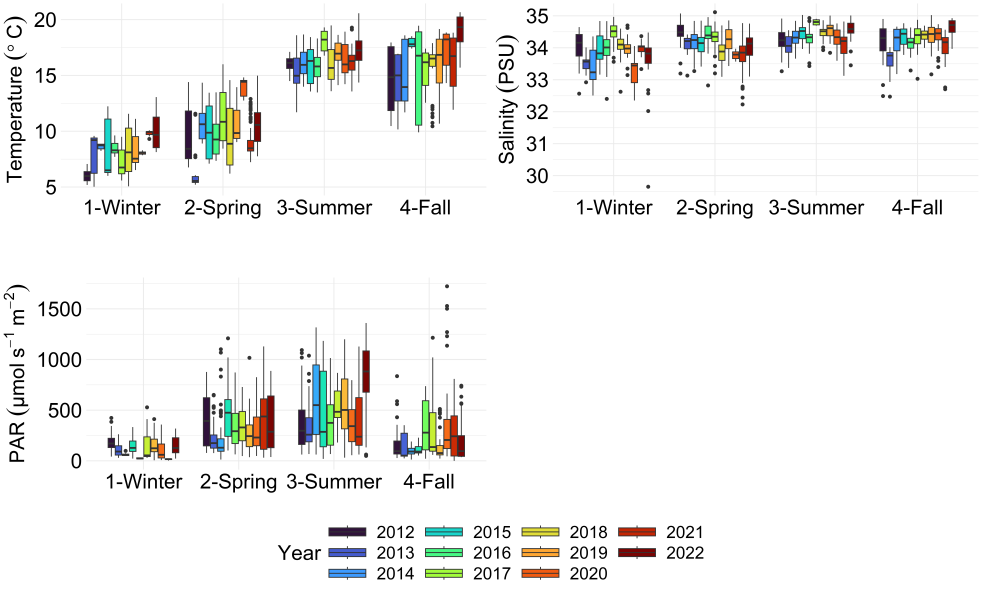

Figure 8. Boxplots of sea surface CTD parameters by season and year along the DYPHYRAD transect from 2011 to 2022. Seasons are defined as winter (December-January-Ferbuary), spring (March-April-May), summer (June-July-August) and fall (September-October-November). The variables represented are temperature, salinity and PAR. The dots indicate outliers. All surface stations were averaged by season.

Nitrate concentrations were very high in fall and winter at the beginning of the series (2012 to 2014), after this period, these values decreased by half. Summer nitrate concentrations were the lowest of the four seasons (0.57 μmol L^{-1}) and a relatively modest maximum (4.34 μmol L^{-1}). However, nitrates were extremely variable in spring, despite the same average as in fall (average: 2.41 μmol L^{-1}), with the highest maximum of the four seasons (55.85 μmol L^{-1}). In fact, Gentilhomme and Lizon (1997) already showed that nitrate stocks are reestablished during the winter period and then decrease during spring bloom until depletion, which explains the dynamics observed in this study and the variability observed during the spring. Spring is characterized by strong variability in nutrient concentrations due to transitional phases before and after phytoplankton blooms. Before the bloom season, nutrient levels are generally higher, whereas after the bloom, depletion occurs due to increased phytoplankton uptake, leading to fluctuating concentrations throughout the season. During this period, phosphorus (P), silicate (Si), and nitrogen (N) are sequentially depleted from late winter to late spring. P is the first to reach limiting concentrations, followed by Si and then N. This depletion pattern supports the persistence of *Phaeocystis* blooms, as these organisms can utilize dissolved organic phosphorus (DOP) and do not require Si for growth (van Boekel et al., 1992; Lancelot et al., 2005; Passow et al., 2007; Chai et al., 2023).

The years with the highest median concentrations were 2018, 2019, 2021 and 2022 for silicates, and 2012 for phosphates, influenced by high winter concentrations (Fig. 9C and D). Phosphate and silicate concentrations were also relatively high in

https://doi.org/10.5194/essd-2025-131
Preprint. Discussion started: 12 March 2025

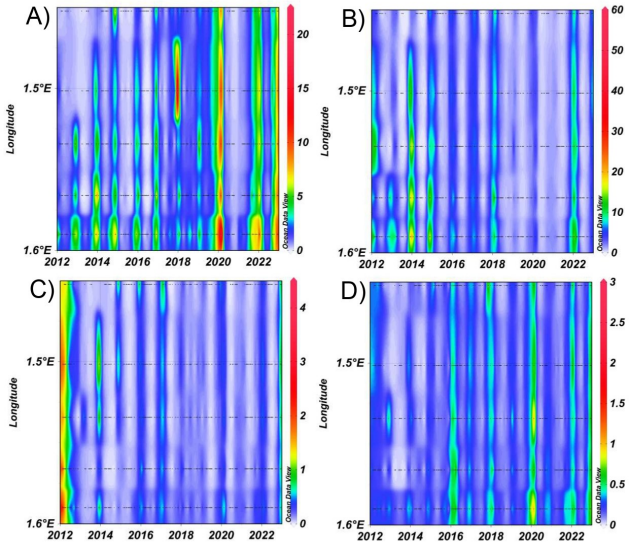

Figure 9. Spatial variability of surface nutrients concentration in μmol L^{-1} over time (2012-2022): (A) nitrate, (B) nitrite, (C) phosphate and (D) silicate along DYPHYRAD transect.

fall with respective mean concentration of 0.22 (min : 0.001; max : 0.837 μmol L^{-1}) and 2.35 μmol L^{-1} (min : 0.001; max : 9.59 μmol L^{-1}). Previous studies showed an increase in nutrient concentration in the waters of EEC and southern North Sea since 1930 (Laane et al., 1993). These nutrient stocks play an important role in the spatio-temporal dynamics of phytoplankton (e.g., diatoms or *Pheaocystis*) (Karasiewicz et al., 2018). Over the past eleven years, phosphate concentrations have tended to rise in fall and winter, and decrease in summer. We hypothesize that increased release of dissolved inorganic phosphorus (DIP) from particulate inorganic phosphorus (PIP) occurs due to adsorption-desorption processes, particularly intensified by storms or heavy rainfall that leach soils during winter and fall. On the other hand, the highest phosphate values were found in winter 2020 with a median of 0.70 μmol L^{-1}. Winter silicate concentration decreased until 2017 and then increased again until the end of the series, and this pattern seems to be similar in fall.

Coastal waters showed the greatest variability in environmental parameters due to their shallower depth, greater surface area for exchange with the atmosphere and the seabed (including suspended particles), and significant freshwater inputs from rivers and runoff. These factors contribute to fluctuating temperature, salinity and nutrient levels, making nearshore coastal ecosystems more dynamic than offshore coastal environments.

https://doi.org/10.5194/essd-2025-131
Preprint. Discussion started: 12 March 2025

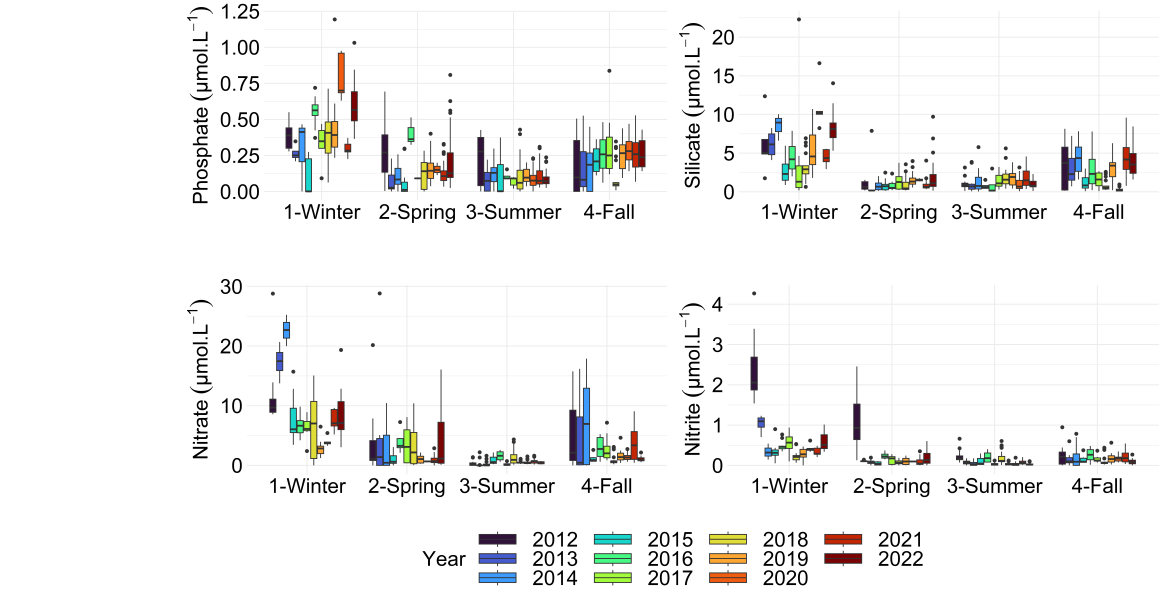

Figure 10. Boxplots of nutrient concentration for each season of each year. The dots indicate outliers. All surface stations were averaged by season

4.2 Phytoplankton measurements: pigment analysis and automated measurement

4.2.1 Total chlorophyll *a* estimated by *in vivo* mono-spectral fluorometry, pigment extraction and FLP Total chlorophyll *a*

The DYPHYRAD transect was subject to seasonal variations in measured and estimated concentration of chlorophyll *a*. Stations nearest the coast had highest values and showed the most marked seasonal variations (Fig. 11). Only years 2013 and 2021 showed a spring bloom that spreads across the entire coastal-offshore transect. This phenomenon was spatially well represented by the three methods. Conversely, some years blooms were concentrated at the coastal station, e.g. from 2016 to 2019, this trend was more marked for the FLP estimation of the total chlorophyll *a* equivalents (Fig. 11C).

As can be seen from median values of these three methods per season (all surface stations were pooled together), the highest values occurred in spring (Fig. 12 and 13), as reported by previous studies (Breton et al., 2000; Schapira et al., 2008; Lefebvre et al., 2011; Belin et al., 2012; Hernandez Farinas et al., 2020). This period is generally favorable for bloom development, as light intensity and photoperiod increase, associated to better weather conditions. In addition, nutrient stocks are relatively high in winter, as phytoplankton growth is limited by reduced light availability. This allows nutrients to accumulate in the water column. The regeneration of nutrient stocks is also due to increased inputs from estuaries, rain and runoff, which transport nutrients of terrestrial origin into the marine system. Spring chlorophyll *a* concentration median values ranged from 1.4 to 6.5 μg L^{-1} (Fig. 12), while *in vivo* chlorophyll *a* fluorescence spring median values ranged between 0.9 and 4.8 FFU (Fig. 13)

https://doi.org/10.5194/essd-2025-131
Preprint. Discussion started: 12 March 2025

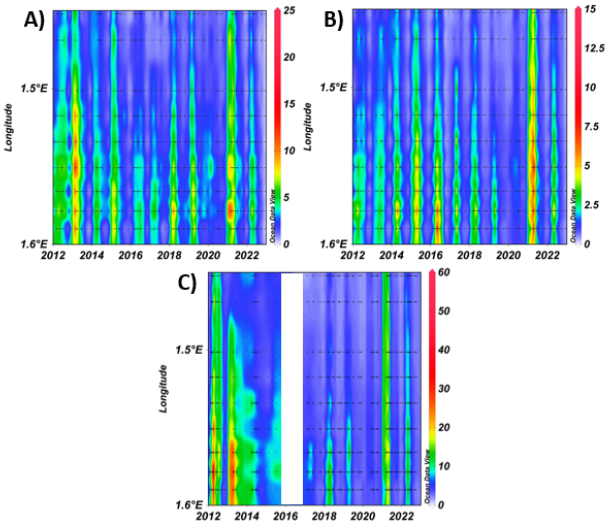

Figure 11. Spatial variability of phytoplankton biomass along the DYPHYRAD transect over time: (A) chlorophyll *a* (μg L^{-1}), (B) *in vivo* total chlorophyll *a* fluorescence (FFU) and (C) FLP Total chlorophyll *a* equivalents (μg chl-*a* Eq. L^{-1})

whereas FLP Total *in vivo* chl-*a* equivalents ranged between 10 and 30 μg chl-*a* Eq. L^{-1} (Fig. 14). During this period, the highest phaeopigment concentrations were recorded, with median values ranging from 0.50 to 2.50 μg chl-*a* Eq. L^{-1}). Chlorophyll *a* and pheopigments concentrations decreased during summer, at different times and magnitude depending on the year. Particularly, intense spring blooms were observed in 2013 and 2021, relaying on chlorophyll *a* concentrations. This trend was well reflected with *in vivo* fluorescence for 2021, but slightly underestimated for 2013 (one of the major spring blooms of the series appeared to be for the year 2014 instead). Other blooms were less intense, either starting in late winter to early spring or beginning later but persisting over a longer period. For instance, in 2016, chlorophyll *a* and *in vivo* fluorescence levels remained relatively stable during both spring and summer, averaging 3.04 μg L^{-1} and 3.48 μg L^{-1} and 3.45 FFU and 1.90 FFU, respectively. By contrast, 2013 or 2017 saw an early bloom, with chlorophyll *a* concentrations averaging 3.87 μg L^{-1} (max : 11.77 μg L^{-1}) and 2.52 μg L^{-1} (max: 6.050 μg L^{-1}) respectively in winter. The timing and intensity of spring blooms (whether early and low or late and high) can be influenced by various factors, including limited light availability caused by turbidity from suspended sediments or competition with diatoms (Guiselin, 2010). Lastly, 2020 was unusual in that very few data were acquired during the spring period because of the pandemic lockdown, so these spring values could not be considered representative of a bloom or only late spring-early summer one. In autumn, average chlorophyll *a* and *in vivo* fluorescence values were low and fairly constant, as reported in previous studies (Lefebvre and Ambiaud, 2017). It would appear that values vary more during the winter period, particularly for pigment extraction method. However, this variability could partly be attributed to a lower sampling rate, as worsening weather heavily impacts sample collection, which is highly dependent on weather conditions.

https://doi.org/10.5194/essd-2025-131
Preprint. Discussion started: 12 March 2025

Open Access Earth System Science Data Discussions

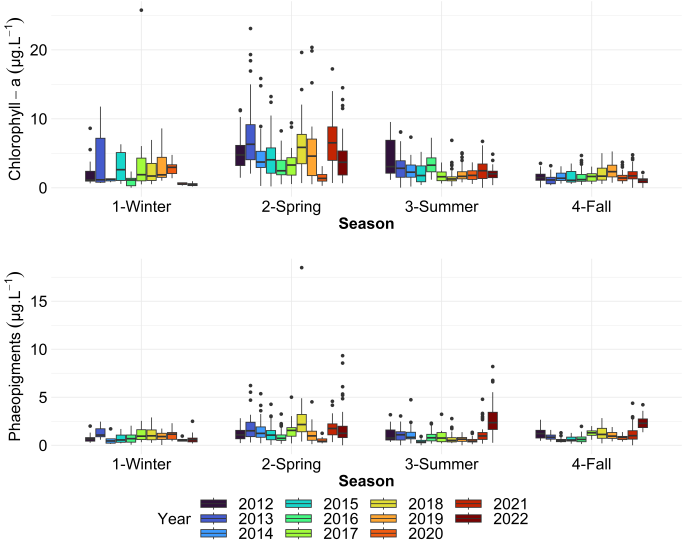

Figure 12. Boxplots of chlorophyll *a* concentration (μg L^{-1}) and Phaeopimgent concentration (μg L^{-1}) for each season of each year along the DYPHYRAD transect. The dots indicate outliers. All surface stations were gathered by season.

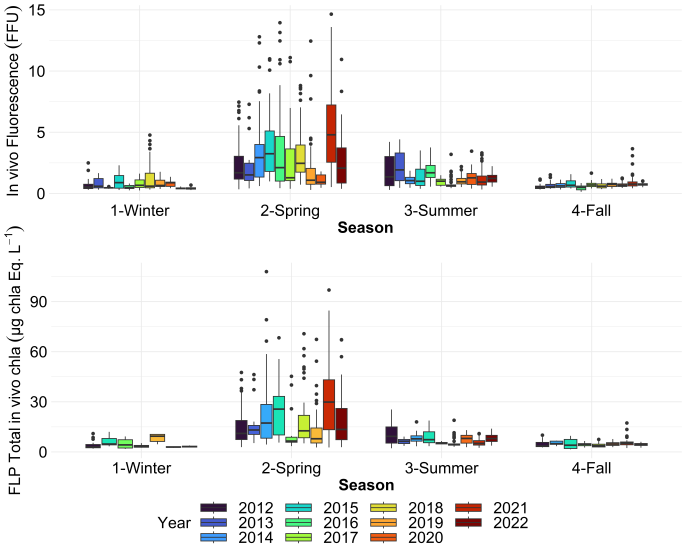

Figure 13. Boxplots of *in vivo* chl-*a* fluorescence (FFU) and FluoroProbe Total chl-*a* estimates (μg chl-*a* Eq. L^{-1}) for each season of each year over the whole DYPHYRAD transect. The dots indicate outliers. All surface stations were gathered by season.

https://doi.org/10.5194/essd-2025-131
Preprint. Discussion started: 12 March 2025

4.2.2 Phytoplankton spectral (pigmentary) groups addressed by *in vivo* multi-spectral fluorometry

Multi-spectral fluorescence enables to differentiate up to four spectral (pigmentary) groups. The seasonal and annual data presented in this study focus on the FluoroProbe TS-16-16 device, as it provided the longest time series with the highest sampling frequency. However, similar data for TS-22-15 is also available in the dataset. The FluoroProbe was used to characterize the phytoplankton community assemblage with three common fingerprints ("brown", "blue-green" and "mix-red") and a choice made between two different fingerprints: Green Algae or *Phaeocystis* (Fig. 14). *Phaeocystis* was the main Haptophyte in our study area (Astoreca et al., 2009; Lefebvre et al., 2011). As a result, seasonal concentrations was represented only for this fingerprint, although the full dataset remains available. Data from TS-22-15 are not represented in this study because the haptophyte fingerprint was obtained in two different ways (local *Phaeocystis* fingerprint, then *Isochrysis* haptophyte fingerprint installed by the manufacturer) and this instrument has been used in a more heterogeneous way (no data between 2017 and 2021).

Fairly marked seasonal variations were observed, as stated in previous studies (Lancelot et al., 1998; Grattepanche et al., 2011) and on the same coastal-offshore transect (Houliez et al., 2013), notably for *Phaeocystis* and Diatoms (Fig. 14). The start of the bloom for "brown algae" (mainly diatoms here) is in winter, with more productive years between 2012 and 2017 (3 μg chl-*a* Eq. L^{-1}). As expected, spring was confirmed to be a productive period for the "brown algae" with particular years like 2017 and 2018 (2.50 μg chl-*a* Eq. L^{-1}). In summer and fall, diatom concentration in chl-*a* equivalents were generally similar, with slightly higher values observed in fall 2014 and 2021 (Fig. 14). Generally, a succession of phytoplankton typical of the EEC is characterized by a late winter or early spring. Diatom bloom followed by a *Phaeocystis* spring bloom (Breton et al., 2000; Guiselin, 2010; Grattepanche et al., 2011). We observed this phenomenon in our time series for years 2012, 2015, 2017 and 2019. Diatoms blooms are linked to the concentration of silicates in the environment, these stocks were high in winter, then decreased during the bloom (Fig. 10) and became a limiting factor (Rousseau et al., 2000). This phenomenon can also be linked to the seasonality of the amount of available light (Peperzak et al., 1998). For *Phaeocystis*, spring was the most productive period, with highest values in 2013 (17 μg chl-*a* Eq. L^{-1}) and 2021 (15 μg chl-*a* Eq. L^{-1}). *Phaeocystis* developed a maximum biomass in spring (Fig. 14) in the English Channel (Belin et al., 2012). It represented between 28 and 90 % of the total chlorophyll *a* estimated *in vivo* over the entire time series (Fig. 15). These blooms are stimulated by nitrate and phosphate enrichment (Lancelot et al., 1998; Lefebvre and Ambiaud, 2017), from nutrient inputs from rivers, exchanges with offshore water masses and with sediment from shallow areas (Reynolds, 2006).

The red-mix algae spectral group (Cryptophyes, cyanobacteria showing Phycoerythrine as major pigment) varied very little throughout the year and were the minority group in our study area, as reported in previous studies, with less than 10 % maximum over 11 years (Fig. 15; Houliez et al., 2013; Lefebvre and Poisson-Caillault, 2019). The "blue-green" group (cyanobacteria of Phycocyanine as major pigment) was highly variable in spring and summer, with concentrations ranging 0 (corresponding to undetected values) to 1 μg chl-*a* Eq. L^{-1}. A marked trend emerged in summer, with a 5-year period of marked increase starting in 2012 with a peak in 2017, followed by a 5-year period of decline until 2022 (Fig. 14). An increase was evidenced in fall from 2017 onward compared with previous years (25 % of total concentration; Fig. 15), then from 2019 the trend was

https://doi.org/10.5194/essd-2025-131
Preprint. Discussion started: 12 March 2025

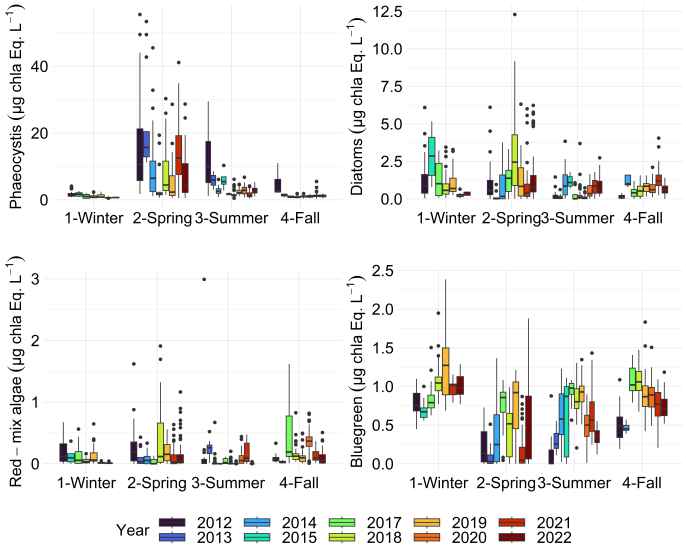

Figure 14. Boxplots of phytoplankton spectral (pigmentary) groups addressed along the DYPHYRAD transect with the Fluoroprobe (including the *Phaeocystis* fingerprint) for each season of each year. The dots indicate outliers. All surface stations were gathered by season

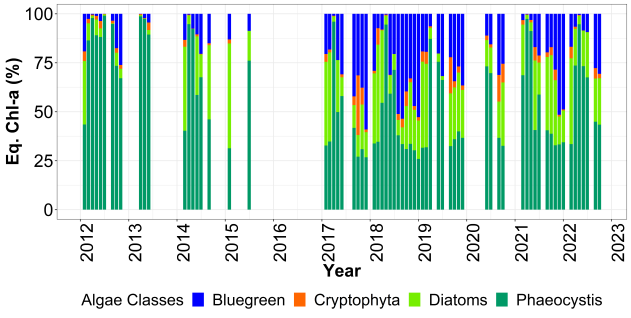

Figure 15. Relative contribution (%) of Fluoroprobe-defined spectral groups along the DYPHYRAD transect to FLP Total chlorophyll *a* estimation, with *Phaeocystis* fingerprint of TS-16-16 device.

downwards for this season. Conversely, in winter over 11 years, this group show an apparent increasing trend between 2015 and 2019, followed by a period of sharp decline in 2021 and 2022.

4.2.3 Abundance and biomass of phytoplankton optical (functional) groups addressed by Automated Flow Cytometry

The variability in phytoplankton groups, analysed through automated flow cytometry, defined pronounced spatial patterns, with
335 OraPicoProk (i.e. *Synechococcus* sp.) showing higher abundances in offshore than in coastal waters (Fig. 16A). The years 2015 to 2018 showed this spatial pattern in particular. The year 2021, on the other hand, showed the highest abundances observed for this group, provoking a less pronounced coast- offshore gradient. For the RedPico (i.e. picoeukaryotes) and OraNano (i.e.

https://doi.org/10.5194/essd-2025-131
Preprint. Discussion started: 12 March 2025

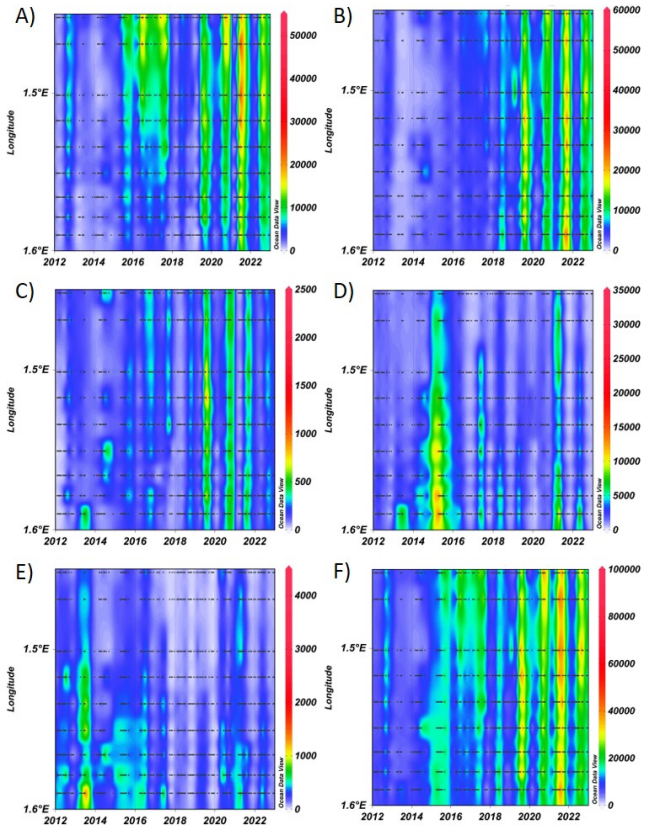

Figure 16. Spatial variability of phytoplankton abundance along the DYPHYRAD trasect, from 2012 to 2022 (cell mL^{-1}): (A) OraPicoProk , (B) RedPico (C) OraNano, (D) RedNano, (E) RedMicro and (F) Total of phytoplancton abundance.

cryptophytes) groups (Fig. 16B and C), there was no coastal-offshore gradient, but an increase in abundance within these groups from year 2019 onwards. The RedNano and RedMicro groups showed higher abundances close to the coast, with a particularly marked bloom in 2015 for RedNano (mainly represented by *Phaeocystis globosa* free flagellates and colonial cells during the spring bloom and other nanoeukaryotes during the rest of the time) and 2013 for RedMicro (i.e. diatoms, pigmented dinoflagellates and, if highly concentrated, *Phaeocystis* colonies). Total abundance showed no regular pattern and seemed to depend on the very high abundance of different groups such as OraPicoProk (Fig. 16F).

Over time, this series allowed to follow the succession of phytoplankton communities, with a clear dominance of OraPicoProk and RedPico, except during the spring when RedNano dominated the community by almost 90 % (Fig. 17). This very large abundance of RedNano in spring corresponded mostly to the well-known *P. globosa* bloom in the area (Breton et al., 2000; Grattepanche et al., 2011; Lefebvre et al., 2011; Breton et al., 2022). Flow cytometry can discriminate its different life stages, allowing haploid, diploid, and colonial cells to be distinguished (Rutten et al., 2005; Guiselin, 2010; Houliez et al., 2012; Bonato et al., 2015) but not shown here. The strongest RedNano spring bloom recorded in the time series was in 2015 with

https://doi.org/10.5194/essd-2025-131
Preprint. Discussion started: 12 March 2025

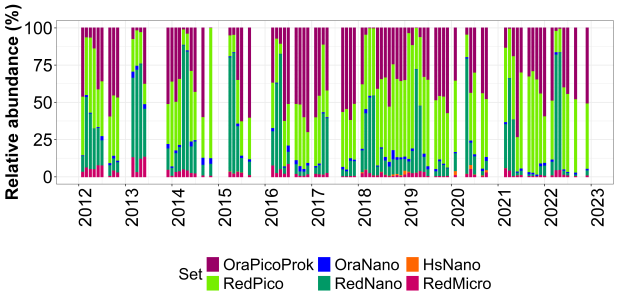

Figure 17. Relative abundance (%) of PFGs over the whole DYPHYRAD transect (average values over the 9 stations), over time (2012-2022).

maximum abundance of 3.20×10^{-4} cell mL^{-1} (R0 station on May 22nd). The summer of 2021 was the most abundant in total phytoplankton cells, largely dominated by the highest abundance of OraPicoProk with an abundance of 5.44×10^{-4} cell mL^{-1} (R1 station on June 23rd). The dominance of OraPicoProk in summer, and particularly in the hottest summers (as in the summer 2022), can be explained by an optimum temperature in the growth rate of *Synnechococcus* spp. at high temperatures (Pittera et al., 2014; Robache et al., in prep). The abundance of RedPico exhibited a clear seasonal variation, with a higher abundance observed during summer and fall (Fig. 18). The peak of RedPico abundance was recorded in summer 2020. A multi-year increase in RedPico and OraPicoProk has already been observed over the last decade (Hubert et al., 2025). In the English Channel, RedPico is predominantly composed of *Chlorophyta* (Marie et al., 2010; Masquelier et al., 2011). The OraNano, HsNano and RedMicro groups made a minimal contribution to total phytoplankton abundance. RedMicro cells (as well as RedNano), though less abundant than smaller cells and responsible for phytoplankton blooms before and after *Phaeocystis globosa* blooms, nevertheless make up a large part of the biovolume, chlorophyll content (FLR, not shown) and biomass in the EEC.

5 Conclusions

The dataset derived from the DYPHYRAD surveys deploying automated *in vivo* measurements at high spatial resolution with innovative optical sensors provided insights into the coastal-offshore phytoplankton variability and weekly, seasonal and inter-annual dynamics for 11 years. These data, addressing phytoplankton functional diversity, should be useful to contribute to the calculation of indicators to describe the state of the pelagic environment (Rombouts et al., 2019), to feed models that could predict algal blooms in the EEC, to study the structure and dynamics of phytoplankton community functional assemblies, and/or to model and improve our understanding of the impact of anthropogenic pressures and climate change on this marine ecosystem. By covering the full phytoplankton size range through *in vivo* automated measurements on a weekly basis and at a fine spatial scale, this approach complements fortnightly to monthly monitoring services and networks. It enables the integration of functional data into trophic models, thereby supporting the management of living resources. This monitoring is

https://doi.org/10.5194/essd-2025-131
Preprint. Discussion started: 12 March 2025

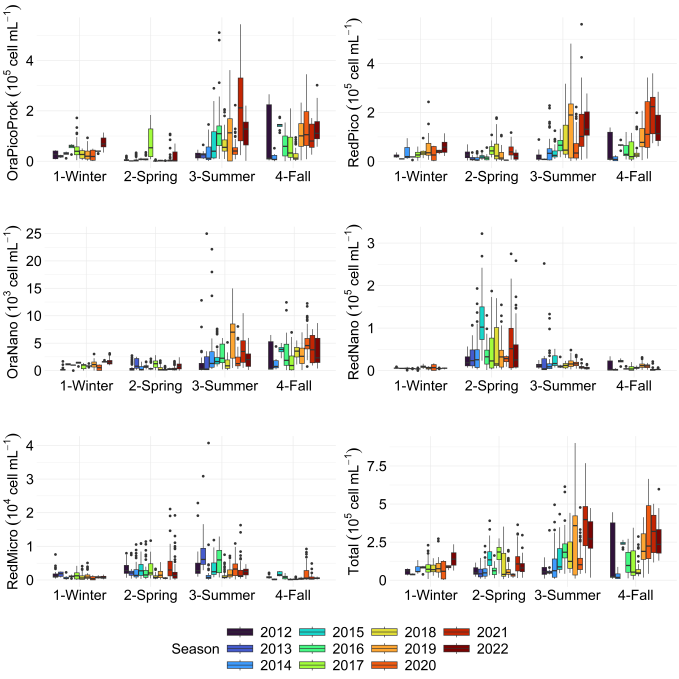

Figure 18. Boxplots of PFGs abundance for each season of each year. The dots indicate outliers.

planned to continue, having been recognized as valuable to the French research community by the IR ILICo, which unites all national observation services. It also holds potential for expansion, including the integration of additional applications such as automated imaging.

6 Data availability

The DYPHYRAD dataset is available at https://doi.org/10.17882/104524 (Hubert et al., 2025).

Appendix A: Sampling coordinates and general statistics of dataset

The Table A1 shows the coordinates of the 9 transect sampling points in decimal degrees. The Table A2 represents the descriptive statistics for the parameters measured during DYPHYRAD cruises from 2012 until 2022. The table shows the number of total discrete measurements made, as well as the distribution of data via median, first and third quartile. The number of missing values is also reported, which may be due to a measurement problem related to the instrument.

https://doi.org/10.5194/essd-2025-131
Preprint. Discussion started: 12 March 2025

Open Access Earth System Science Data Discussions

Table A1. Coordinates of DYPHYRAD transect stations.

Station	Longitude	Latitude
R0	1.5900	50.8
R0'	1.5786	50.8
R1	1.5660	50.8
R1'	1.5508	50.8
R2	1.5342	50.8
R2'	1.5175	50.8
R3	1.5014	50.8
R3'	1.4690	50.8
R4	1.4522	50.8

Table A2. Descriptive information of the dataset: the size (n), minimum and maximum values (Min and Max), first and third quartiles (Q1 and Q3), median, mean and number of missing data (NAs).

Parameters (Units)	n	Min	Q1	Median	Mean	Q3	Max	NAs
Temperature (°C)	1,766	5.03	9.15	13.34	12.90	16.53	20.66	69
Salinity (PSU)	1,728	29.65	33.96	34.28	34.20	34.51	35.11	107
PAR (μmol s^{-1} m^{-2})	1,588	0.08	108.41	228.53	335.37	503.45	1,722.56	247
CTD Fluorescence (FFU)	783	0.03	0.39	1.49	5.48	4.71	131.52	1,052
Nitrate + Nitrite (μmol L^{-1})	1,021	0.002	0.42	1.02	2.69	3.13	57.15	814
Phosphate (μmol L^{-1})	1,024	0.001	0.07	0.14	0.20	0.27	2.96	811
Silicate (μmol L^{-1})	1,017	0.001	0.13	0.78	1.73	2.31	22.29	818
Chlorophyll *a* (μg L^{-1})	1,773	0	1.25	2.22	3.11	4.06	25.75	62
Phaeopigment (μg L^{-1})	1,773	0	0.54	0.90	1.19	1.53	18.50	62
TD-10AU *in vivo* fluorescence (FFU)	1,820	0.13	0.62	1.01	1.77	1.98	14.65	15
FLP Total chlorophyll *a* (μg chl-*a* Eq. L^{-1})	1,189	1.58	4.28	6.55	11.44	11.90	107.92	646
FCM Cell abundance (cell mL^{-1})	1,522	145.80	5,043.50	9,251.40	14,200.20	18,985.20	90,071.30	313

Appendix B: FluoroProbe green algae fingerprint

The FluoroProbe was also used to characterize the assembly of the phytoplankton community in complement of previous results obtain with *Phaeocystis* fingerprint (shown in the main results section of the paper) with common fingerprints based on that defined by the manufacturer "brown", "blue-green" and "red-mix" and "green algae" (Fig. B1 and B2).

https://doi.org/10.5194/essd-2025-131
Preprint. Discussion started: 12 March 2025

Open Access Earth System Science Data Discussions

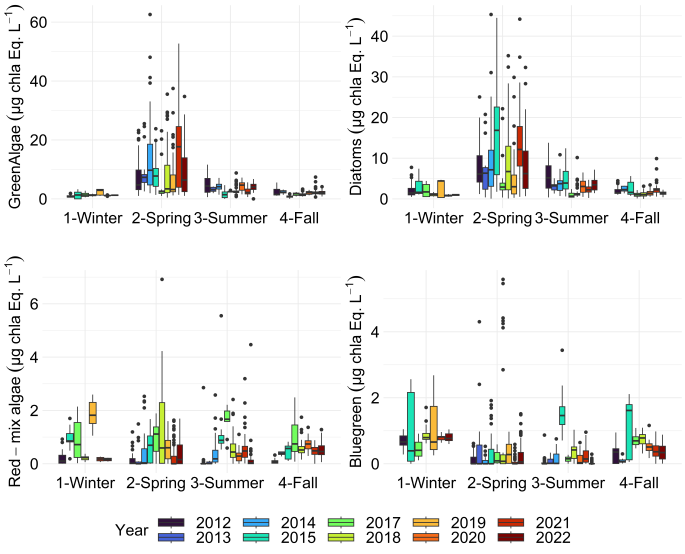

Figure B1. Boxplots of phytoplankton spectral (pigmentary) groups addressed with Fluoroprobe TS-16-16 (including the *Green algae* manufacturer fingerprint) for each season of each year. The dots indicate outliers. All surface stations were gathered by season.

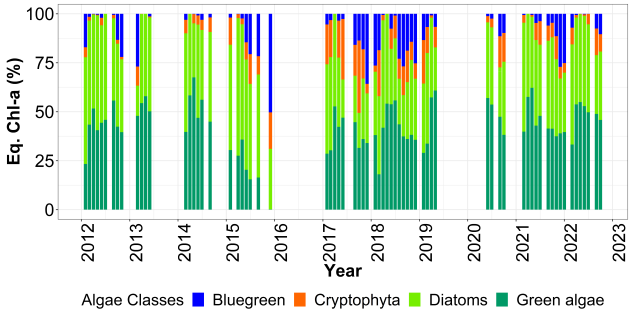

Figure B2. Relative contribution (%) of Fluoroprobe-defined spectral groups to FLP Total chlorophyll *a* estimation, with *Green algae* fingerprint of TS-16-16 device along the DYPHYRAD transect, from 2012 to 2022.

https://doi.org/10.5194/essd-2025-131
Preprint. Discussion started: 12 March 2025

Open Access Earth System Science Data Discussions

Author contributions. LFA conceived and designed the study sampling and applied for different funding source through conventions and projects. ZH, AL, CG, VC, MC, EL, LFA contributed to data collection and sampling analysis. ZH, AL and CG performed the final data set generation and data analysis. ZH, AL, and CG wrote the original draft and all the authors edited the final version.

Competing interests. The contact authors have declared that none of the authors has any competing interests.

Acknowledgements. We would like to thank the crew (Grégoire Leignel, Christophe Routtier and Noël Lefilliatre) of the research vessel *Sepia II* (CNRS INSU-FOF). We also thank Morgane Didry, Jessica Delarbre, Claire Dedecker, Marie Bruaut, Emeline Lebourg, and Elise Caillard as well as all the intern students, technicians, engineers, and researchers hired on supporting projects who have been on board to carry out sea sampling along the DYPHYRAD transect over the past decade. We would like to thank Fabrice Lizon, who ensured the continuity of multi-spectral fluorescence measurements in parallel with primary production measurements. We thank the funding projects DYMAPHY INTERREG-IV A "2 Seas", French State – ERDF - Nord-Pas-de-Calais Hauts-de-France Regional Projects (CPER) "*Phaeocystis* Bloom", MARCO, IDEAL, the CNRS-IFREMER WFD convention, JERICO NEXT and JERICO S3 H2020 INFRAIA projects, CNRS INSU-MTES Convention for the implementation of the MSFD, CNRS-Water Agency Artois Picardie convention, with their respective funding bodies (French State, Nord-Pas-de-Calais and Hauts de France Regions, the European Commission). ZH was supported by a Doctorate (Ph.D.) grant from the "Hauts-de-France" Region and the University of Littoral Côte d'Opale (ULCO) at the Doctoral School ED STS (UPJV, UA, ULCO). This work is also supported by the Priority Research Project "Ocean and Climate" PPR RiOMar (2022-2028) supported by a France 2030 grant (ANR-22-POE-0006), the Graduate School IFSEA that also benefits from a France 2030 grant (ANR-21-EXES-0011) operated by the French National Research Agency and the OBAMA NEXT (2022-2026) project (Horizons-CL6-2022-BIODIV-01-01).

https://doi.org/10.5194/essd-2025-131
Preprint. Discussion started: 12 March 2025

References

Aminot, A. and Kérouel, R.: Dosage automatique des nutriments dans les eaux marines: méthodes en flux continu, Editions Quae, ISBN 978-2-7592-0023-8, 2007.

Astoreca, R., Rousseau, V., and Lancelot, C.: Coloured dissolved organic matter (CDOM) in Southern North Sea waters: Optical characterization and possible origin, Estuarine, Coastal and Shelf Science, 85, 633–640, 2009.

Auber, A., Gohin, F., Goascoz, N., and Schlaich, I.: Decline of cold-water fish species in the Bay of Somme (English Channel, France) in response to ocean warming, Estuarine, Coastal and Shelf Science, 189, 189–202, 2017.

Belin, C., Haberkorn, H., and Menesguen, A.: Communautés du phytoplancton. Sous-région marine Manche-Mer du Nord. Evaluation initiale DCSMM., 2012.

Bentley, D., Lafite, R., Morley, NH., James, R., Statham, PJ., and Guary, JC.: Flux de Nutriments Entre La Manche et La Mer Du Nord. Situation Actuelle et Évolution Depuis Dix Ans, Oceanologica Acta, 16, 599–606, 1993.

Berglund, J., Müren, U., Båmstedt, U., and Andersson, A.: Efficiency of a Phytoplankton-Based and a Bacterial-Based Food Web in a Pelagic Marine System, Limnology and Oceanography, 52, 121–131, https://doi.org/10.4319/lo.2007.52.1.0121, 2007.

Beutler, M., Wiltshire, K. H., Meyer, B., Moldaenke, C., Lüring, C., Meyerhöfer, M., Hansen, U.-P., and Dau, H.: A fluorometric method for the differentiation of algal populations in vivo and in situ, Photosynthesis research, 72, 39–53, 2002.

Bierman, P., Lewis, M., Ostendorf, B., and Tanner, J.: A Review of Methods for Analysing Spatial and Temporal Patterns in Coastal Water Quality, Ecological Indicators, 11, 103–114, https://doi.org/10.1016/j.ecolind.2009.11.001, 2011.

Bonato, S., Christaki, U., Lefebvre, A., Lizon, F., Thyssen, M., and Artigas, L. F.: High Spatial Variability of Phytoplankton Assessed by Flow Cytometry, in a Dynamic Productive Coastal Area, in Spring: The Eastern English Channel, Estuarine, Coastal and Shelf Science, 154, 214–223, https://doi.org/10.1016/j.ecss.2014.12.037, 2015.

Breton, E., Brunet, C., Sautour, B., and Brylinski, J.-M.: Annual Variations of Phytoplankton Biomass in the Eastern English Channel: Comparison by Pigment Signatures and Microscopic Counts, Journal of Plankton Research, 22, 1423–1440, https://doi.org/10.1093/plankt/22.8.1423, 2000.

Breton, E., Goberville, E., Sautour, B., Ouadi, A., Skouroliakou, D.-I., Seuront, L., Beaugrand, G., Kléparski, L., Crouvoisier, M., Pecqueur, D., Salmeron, C., Cauvin, A., Poquet, A., Garcia, N., Gohin, F., and Christaki, U.: Multiple Phytoplankton Community Responses to Environmental Change in a Temperate Coastal System: A Trait-Based Approach, Frontiers in Marine Science, 9, https://doi.org/10.3389/fmars.2022.914475, 2022.

Brylinski, J. M., Lagadeuc, Y., Gentilhomme, V., Dupont, J. P., Lafite, R., Dupeuble, P. A., Huault, M. F., and Auger, Y.: Le "fleuve côtier" : Un phénomène hydrologique important en Manche orientale. Exemple du Pas-de-Calais, Oceanologica Acta, Special issue, 1991.

Cadée, G. C. and Hegeman, J.: Phytoplankton in the Marsdiep at the end of the 20th century; 30 years monitoring biomass, primary production, and Phaeocystis blooms, Journal of Sea Research, 48, 97–110, 2002.

Chai, X., Zheng, L., Liu, J., Zhan, J., and Song, L.: Comparison of Photosynthetic Responses between Haptophyte Phaeocystis Globosa and Diatom Skeletonema Costatum under Phosphorus Limitation, Frontiers in Microbiology, 14, https://doi.org/10.3389/fmicb.2023.1085176, 2023.

Desmit, X., Nohe, A., Borges, A. V., Prins, T., De Cauwer, K., Lagring, R., Van der Zande, D., and Sabbe, K.: Changes in chlorophyll concentration and phenology in the North Sea in relation to de-eutrophication and sea surface warming, Limnology and Oceanography, 65, 828–847, 2020.

https://doi.org/10.5194/essd-2025-131
Preprint. Discussion started: 12 March 2025

Dulière, V., Gypens, N., Lancelot, C., Luyten, P., and Lacroix, G.: Origin of nitrogen in the English Channel and Southern Bight of the North Sea ecosystems, Hydrobiologia, 845, 13–33, 2019.

Fontana, S., Jokela, J., and Pomati, F.: Opportunities and Challenges in Deriving Phytoplankton Diversity Measures from Individual Trait-Based Data Obtained by Scanning Flow-Cytometry, Frontiers in Microbiology, 5, https://doi.org/10.3389/fmicb.2014.00324, 2014.

Fragoso, G. M., Poulton, A. J., Pratt, N. J., Johnsen, G., and Purdie, D. A.: Trait-Based Analysis of Subpolar North Atlantic Phytoplankton and Plastidic Ciliate Communities Using Automated Flow Cytometer, Limnology and Oceanography, 64, 1763–1778, https://doi.org/10.1002/lno.11189, 2019.

Galvin, J.: The storms of February 2020 in the channel islands and south west England, Weather, 77, 43–48, 2022.

Gentilhomme, V. and Lizon, F.: Seasonal cycle of nitrogen and phytoplankton biomass in a well-mixed coastal system (Eastern English Channel), Hydrobiologia, 361, 191–199, 1997.

Giering, S. and Humphreys, M.: Biological Pump, in: Encyclopedia of Earth Sciences Series, https://doi.org/10.1007/978-3-319-39193-9_154-1, 2017.

Girardin, R., Vermard, Y., Thébaud, O., Tidd, A., and Marchal, P.: Predicting fisher response to competition for space and resources in a mixed demersal fishery, Ocean & Coastal Management, 106, 124–135, 2015.

Grattepanche, J.-D., Breton, E., Brylinski, J.-M., Lecuyer, E., and Christaki, U.: Succession of Primary Producers and Micrograzers in a Coastal Ecosystem Dominated by Phaeocystis Globosa Blooms, Journal of Plankton Research, 33, 37–50, https://doi.org/10.1093/plankt/fbq097, 2011.

Guinaldo, T., Voldoire, A., Waldman, R., Saux Picart, S., and Roquet, H.: Response of the sea surface temperature to heatwaves during the France 2022 meteorological summer, Ocean Science, 19, 629–647, 2023.

Guiselin, N.: Etude de La Dynamique Des Communautés Phytoplanctoniques Par Microscopie et Cytométrie En Flux, En Eaux Côtière de La Manche Orientale, These de doctorat, Littoral, 2010.

Haraguchi, L., Jakobsen, H. H., Lundholm, N., and Carstensen, J.: Monitoring Natural Phytoplankton Communities: A Comparison between Traditional Methods and Pulse-Shape Recording Flow Cytometry, Aquatic Microbial Ecology, 80, 77–92, https://doi.org/10.3354/ame01842, 2017.

Hernandez Farinas, T., Menet-Nedelec, F., M Zari, L., Courtay, G., Lampert, L., M Zari, L., Courtay, G., and Lampert, L.: Etude de la dynamique et de la composition du phytoplancton via l'approche des pigments appliquée au littoral normand, Tech. rep., Ifremer, 2020.

Holm-Hansen, O., Lorenzen, C. J., Holmes, R. W., and Strickland, J. D. H.: Fluorometric Determination of Chlorophyll, ICES Journal of Marine Science, 30, 3–15, https://doi.org/10.1093/icesjms/30.1.3, 1965.

Houliez, E., Lizon, F., Thyssen, M., Artigas, L. F., and Schmitt, F. G.: Spectral Fluorometric Characterization of Haptophyte Dynamics Using the FluoroProbe: An Application in the Eastern English Channel for Monitoring Phaeocystis Globosa, Journal of Plankton Research, 34, 136–151, https://doi.org/10.1093/plankt/fbr091, 2012.

Houliez, E., Lizon, F., Artigas, L. F., Lefebvre, S., and Schmitt, F. G.: Spatio-temporal variability of phytoplankton photosynthetic activity in a macrotidal ecosystem (the Strait of Dover, eastern English Channel), Estuarine, Coastal and Shelf Science, 129, 37–48, 2013.

Hubert, Z., Libeau, A., Gallot, C., and Artigas, L. F.: Dynamics of Phytoplankton on RADiale of the Saint-Jean Bay (DYPHYRAD) Surveys, https://doi.org/10.17882/104524, 2025.

Kang, Y., Moon, C.-H., Kim, H.-J., Yoon, Y. H., and Kang, C.-K.: Water quality improvement shifts the dominant phytoplankton group from cryptophytes to diatoms in a coastal ecosystem, Frontiers in Marine Science, 8, 710 891, 2021.

https://doi.org/10.5194/essd-2025-131
Preprint. Discussion started: 12 March 2025

Karasiewicz, S., Breton, E., Lefebvre, A., Farinas, T. H., and Lefebvre, S.: Realized niche analysis of phytoplankton communities involving HAB: Phaeocystis spp. as a case study, Harmful Algae, 72, 1–13, 2018.

Laane, R., Groeneveld, G., Devries, A., Vanbennekom, J., and Sydow, S.: Nutrients (P, N, Si) in the channel and the dover strait-seasonal and year-to-year variation and fluxes to the north-sea, in: Oceanologica Acta, vol. 16, pp. 607–616, Gauthier-Villars, 1993.

Lancelot, C., Wassmann, P., and Barth, H.: Ecology of Phaeocystis-dominated ecosystems, Journal of marine systems, 5, 1–4, 1994.

Lancelot, C., Keller, M., Rousseau, V., Smith Jr, W. O., and Mathot, S.: Autoecology of the marine haptophyte Phaeocystis sp., in: Physiological Ecology of Harmful Algal Blooms, 1, pp. 209–224, Springer, 1998.

Lancelot, C., Spitz, Y., Gypens, N., Ruddick, K., Becquevort, S., Rousseau, V., Lacroix, G., and Billen, G.: Modelling Diatom and Phaeocystis Blooms and Nutrient Cycles in the Southern Bight of the North Sea: The MIRO Model, Marine Ecology Progress Series, 289, 63–78, https://doi.org/10.3354/meps289063, 2005.

Lazure, P. and Desmare, S.: Courantologie. Sous-région marine Manche-Mer du Nord. Evaluation initiale DCSMM., 2012.

Lefebvre, A. and Ambiaud, A.: Résultats de la mise en oeuvre des réseaux REPHY et SRN–Zones côtières de la Manche orientale et de la baie sud de la Mer du Nord–Bilan de l'année 2016., 2017.

Lefebvre, A. and Delpech, J.-P.: Le bloom de Phaeocystis en Manche orientale. Nuisances socio-économiques et / ou écologiques ?, 2004.

Lefebvre, A. and Poisson-Caillault, E.: High resolution overview of phytoplankton spectral groups and hydrological conditions in the eastern English Channel using unsupervised clustering, Marine Ecology Progress Series, 608, 73–92, 2019.

Lefebvre, A., Guiselin, N., Barbet, F., and Artigas, F. L.: Long-Term Hydrological and Phytoplankton Monitoring (1992–2007) of Three Potentially Eutrophic Systems in the Eastern English Channel and the Southern Bight of the North Sea, ICES Journal of Marine Science, 68, 2029–2043, https://doi.org/10.1093/icesjms/fsr149, 2011.

Li, D., Xue, Y., Song, Q., Cui, F., Ma, Y., Tong, M., and Shen, P.: First report on large-scale Phaeocystis globosa bloom in the southern Yellow Sea, China, Frontiers in Marine Science, 9, 880 984, 2022.

Lorenzen, C. J.: Determination of Chlorophyll and Pheo-Pigments: Spectrophotometric Equations1, Limnology and Oceanography, 12, 343–346, https://doi.org/10.4319/lo.1967.12.2.0343, 1967.

Marie, D., Shi, X. L., Rigaut-Jalabert, F., and Vaulot, D.: Use of Flow Cytometric Sorting to Better Assess the Diversity of Small Photosynthetic Eukaryotes in the English Channel, FEMS Microbiology Ecology, 72, 165–178, https://doi.org/10.1111/j.1574-6941.2010.00842.x, 2010.

Masquelier, S., Foulon, E., Jouenne, F., Ferréol, M., Brussaard, C. P. D., and Vaulot, D.: Distribution of Eukaryotic Plankton in the English Channel and the North Sea in Summer, Journal of Sea Research, 66, 111–122, https://doi.org/10.1016/j.seares.2011.05.004, 2011.

Medlin, L. and Zingone, A.: A taxonomic review of the genus Phaeocystis, vol. 83, ISBN 978-1-4020-6213-1, https://doi.org/10.1007/978-1-4020-6214-8_2, 2007.

Passow, U., Rocha, C. L. D. L., Arnosti, C., Grossart, H.-P., Murray, A. E., and Engel, A.: Microbial Dynamics in Autotrophic and Heterotrophic Seawater Mesocosms. I. Effect of Phytoplankton on the Microbial Loop, Aquatic Microbial Ecology, 49, 109–121, https://doi.org/10.3354/ame01138, 2007.

Peperzak, L. and van Wezel, R.: Human Fatalities Related to a *Phaeocystis* Harmful Algal Bloom in the North Sea, Harmful Algae, 130, 102 545, https://doi.org/10.1016/j.hal.2023.102545, 2023.

Peperzak, L., Colijn, F., Gieskes, W., and Peeters, J.: Development of the diatom-Phaeocystis spring bloom in the Dutch coastal zone of the North Sea: the silicon depletion versus the daily irradiance threshold hypothesis, Journal of Plankton Research, 20, 517–537, 1998.

https://doi.org/10.5194/essd-2025-131
Preprint. Discussion started: 12 March 2025

Pittera, J., Humily, F., Thorel, M., Grulois, D., Garczarek, L., and Six, C.: Connecting Thermal Physiology and Latitudinal Niche Partitioning in Marine Synechococcus, The ISME Journal, 8, 1221–1236, https://doi.org/10.1038/ismej.2013.228, 2014.

Reynolds, C. S.: The ecology of phytoplankton, Cambridge University Press, 2006.

Robache, K., Hubert, Z., Gallot, C., Epinoux, A., Louchart, A. P., Facq, J.-V., Lefebvre, A., Répécaud, M., Cornille, V., Verhaeghe, F., Audinet, Y., Brutier, L., Schmitt, F. G., and Artigas, L. F.: Multi-scale phytoplankton dynamics in a coastal system of the Eastern English Channel: the Boulogne-sur-Mer coastal area, in prep.

Rombouts, I., Simon, N., Aubert, A., Cariou, T., Feunteun, E., Guérin, L., Hoebeke, M., McQuatters-Gollop, A., Rigaut-Jalabert, F., and Artigas, L. F.: Changes in Marine Phytoplankton Diversity: Assessment under the Marine Strategy Framework Directive, Ecological Indicators, 102, 265–277, https://doi.org/10.1016/j.ecolind.2019.02.009, 2019.

Rousseau, V., Becquevort, S., Parent, J.-Y., Gasparini, S., Daro, M.-H., Tackx, M., and Lancelot, C.: Trophic efficiency of the planktonic food web in a coastal ecosystem dominated by Phaeocystis colonies, Journal of Sea Research, 43, 357–372, 2000.

Rousseaux, C. S. and Gregg, W. W.: Interannual Variation in Phytoplankton Primary Production at A Global Scale, Remote Sensing, 6, 1–19, https://doi.org/10.3390/rs6010001, 2014.

Ruela, R., Sousa, M., DeCastro, M., and Dias, J.: Global and regional evolution of sea surface temperature under climate change, Global and Planetary Change, 190, 103 190, 2020.

Rutten, T. P. A., Sandee, B., and Hofman, A. R. T.: Phytoplankton Monitoring by High Performance Flow Cytometry: A Successful Approach?, Cytometry Part A, 64A, 16–26, https://doi.org/10.1002/cyto.a.20106, 2005.

Salmaso, N. and Tolotti, M.: Phytoplankton and anthropogenic changes in pelagic environments, Hydrobiologia, 848, 251–284, 2021.

Saulquin, B. and Gohin, F.: Mean seasonal cycle and evolution of the sea surface temperature from satellite and in situ data in the English Channel for the period 1986–2006, International Journal of Remote Sensing, 31, 4069–4093, 2010.

Schapira, M., Vincent, D., Gentilhomme, V., and Seuront, L.: Temporal Patterns of Phytoplankton Assemblages, Size Spectra and Diversity during the Wane of a Phaeocystis Globosa Spring Bloom in Hydrologically Contrasted Coastal Waters, Journal of the Marine Biological Association of the United Kingdom, 88, 649–662, https://doi.org/10.1017/S0025315408001306, 2008.

Skouroliakou, D.-I., Breton, E., Irion, S., Artigas, L. F., and Christaki, U.: Stochastic and Deterministic Processes Regulate Phytoplankton Assemblages in a Temperate Coastal Ecosystem, Microbiology Spectrum, 10, e02 427–22, https://doi.org/10.1128/spectrum.02427-22, 2022.

Skouroliakou, D.-I., Breton, E., and Christaki, U.: Phaeocystis globosa and Diatom Blooms Promote Distinct Bacterial Communities and Associations in a Coastal Ecosystem, Environmental Microbiology Reports, 16, e13 313, https://doi.org/10.1111/1758-2229.13313, 2024.

Taylor, A., Reid, P., Marsh, T., Jonas, T., and Stephens, J.: Year-to-year changes in the salinity of the eastern English Channel, 1948–1973: a budget, Journal of the Marine Biological Association of the United Kingdom, 61, 489–507, 1981.

Thiébaut, M. and Sentchev, A.: Tidal Stream Resource Assessment in the Dover Strait (Eastern English Channel), International Journal of Marine Energy, 16, 262–278, https://doi.org/10.1016/j.ijome.2016.08.004, 2016.

Thyssen, M., Grégori, G., Créach, V., Lahbib, S., Dugenne, M., Aardema, H. M., Artigas, L.-F., Huang, B., Barani, A., Beaugeard, L., Bellaaj-Zouari, A., Beran, A., Casotti, R., Del Amo, Y., Denis, M., Dubelaar, G. B. J., Endres, S., Haraguchi, L., Karlson, B., Lambert, C., Louchart, A., Marie, D., Moncoiffé, G., Pecqueur, D., Ribalet, F., Rijkeboer, M., Silovic, T., Silva, R., Marro, S., Sosik, H. M., Sourisseau, M., Tarran, G., Van Oostende, N., Zhao, L., and Zheng, S.: Interoperable Vocabulary for Marine Microbial Flow Cytometry, Frontiers in Marine Science, 9, https://doi.org/10.3389/fmars.2022.975877, 2022.

https://doi.org/10.5194/essd-2025-131
Preprint. Discussion started: 12 March 2025

van Boekel, W. H. M., Hansen, F. C., Riegman, R., and Bak, R. P. M.: Lysis-Induced Decline of a Phaeocystis Spring Bloom and Coupling with the Microbial Foodweb, Marine Ecology Progress Series, 81, 269–276, 1992.

Wang, X., Du, D., and Peng, Y.: Assessing the Importance of the Marine Chokepoint: Evidence from Tracking the Global Marine Traffic, Sustainability, 16, 384, 2023.

555 Wong, A., Keeley, R., Carval, T., and Team, A. D. M.: Argo Quality Control Manual for CTD and Trajectory Data, 2019.